Acta Cryst. (1995). B51, 167–174

Structure of Pentakis(methylammonium) Undecachlorodibismuthate(III), $[NH_3(CH_3)]_5Bi_2Cl_{11}$, at 130 K and Mechanism of the Phase Transitions

BY P. CARPENTIER AND J. LEFEBVRE

Laboratoire de Dynamique et Structures des Matériaux Moléculaires (CNRS, URA 801), UFR de Physique, Université de Lille I, 59655 Villeneuve d'Ascq CEDEX, France

AND R. JAKUBAS

Institute of Chemistry of Wroclaw, Juliot Curie Street 14, 50 383 Wroclaw, Poland

(*Received 26 October 1993; accepted 4 February 1994*)

Abstract

Pentakis(methylammonium) undecachlorodibismuthate(III), $[NH_3(CH_3)]_5Bi_2Cl_{11}$, PMACB, at 130 K has the monoclinic structure (MLT). In the low-temperature phase, all the methylammonium cations are ordered (the C—N axes are fixed) and hydrogen bonded by weak N—H···Cl interactions, with distances between 3.04 and 3.42 Å. In comparison to the orthorhombic room-temperature phase (ORT), in the MLT phase one can observe only a change in the torsion angle of bioctahedra units without any essential distortion of the $BiCl_6$ octahedra. The temperature evolution of the monoclinic angle showed that PMACB displays a continuous and subtle orthorhombic→monoclinic ($Pca2_1 \rightarrow P2_1$) transition of *ca* 250 ± 10 K. The change in volume of the unit cell around 170 K corroborated the presence of a structural anomaly. It was suggested that the 170 K anomaly is not accompanied by a change in the space group. Analysis of the disordering of the methylammonium cations between 349 and 130 K indicates the leading role played by the methylammonium cations (12) and (22) in the low-temperature transitions at 250 and 170 K. The crystal data of the low-temperature modifications at 130 K are: M_r = 968.3, monoclinic, $P2_1$, a = 12.880 (4), b = 13.916 (3), c = 15.059 (1) Å, γ = 90.13°, Z = 4, V = 2699 (1) Å^3, D_x = 2.383 Mg m^{-3}, λ(Mo $K\alpha$) = 0.7107 Å, μ = 140.878 cm^{-1}, R = 0.031 for 5931 observed reflections [$I > 3\sigma(I)$].

1. Introduction

$[NH_3(CH_3)]_5Bi_2Cl_{11}$ (PMACB) belongs to a rich family of alkylammonium halogenoantimonate(III) and bismuthate(III) crystals showing interesting polar properties (Jakubas & Sobczyk, 1990). A single-crystal X-ray diffraction study showed that PMACB undergoes a $Pcab \rightarrow Pca2_1$ ferroelectric phase transition between a centrosymmetric orthorhombic high-temperature phase (OHT) and a non-centrosymmetric orthorhombic room-temperature phase (ORT) at 307 K (Jakubas, Sobczyk & Lefebvre, 1989; Lefebvre, Carpentier & Jakubas, 1991). This transition is believed to be connected to the reorientational motion (180° flips) of only one of the five inequivalent methylammonium cations (type 3). The order–disorder mechanism of the ferro-paraelectric transition at 307 K has been confirmed by dielectric dispersion (Pawlaczyk *et al.*, 1992; Iwata & Ishibashi, 1990) and Raman studies (Carpentier, Lefebvre & Jakubas, 1992; Kuok, Ng, Iwata & Ishibashi, 1993). The structure determinations also show that two disordered methylammonium cations (type 2) exist in the unit cell below 307 K. The title crystal experiences an additional physical anomaly on cooling the temperature, at *ca* 170 K, recorded by numerous experimental techniques (Mroz & Jakubas, 1990; Pawlowski, Ramos & Cerro, 1993) and it was interpreted as a continuous phase transition. This transition is believed to be related to the dynamics of the methylammonium cations (Type 2). However, a recent study of PMACB under a polarizing microscope (Iwata & Ishibashi, 1992) did not confirm the existence of the expected ferroelastic phase transition around 170 K.

It was not clear whether the 170 K anomaly exists in thermal expansion. It is the aim of this paper to show the existence of structural transformations in the low-temperature region between 270 and 100 K. In this paper, the structure of the monoclinic low-temperature phase (MLT) of PMACB at 130 K is presented. The disorder of the methylammonium cations in different phases (OHT, ORT, MLT) is compared and the mechanism of the successive phase transitions is discussed.

2. Experimental

$[NH_3(CH_3)]_5Bi_2Cl_{11}$ was synthesized and prepared for the X-ray studies using the method described earlier by Lefebvre, Carpentier & Jakubas (1991).

© 1995 International Union of Crystallography
Printed in Great Britain – all rights reserved

The unit-cell parameters were refined using a least-squares fit on the positions of 25 reflections. The monoclinic symmetry was found. Taking the same notation for the crystallographic axes as for the ORT phase, the monoclinic angle found between axes a and b is noticed in the text as the γ angle. The monoclinic symmetry is very close to orthorhombic and the γ angle was found to be 90.13°. The h,k,l reflections with the conditions $0kl$, $l = 2n + l$ and $h0l$, $h = 2n + l$, which are systematic extinctions in ORT, become observed reflections in MLT. From the observed systematic extinctions 001, $l = 2n + l$, the only possible space group, $P2_1$, in MLT (as a subgroup of $Pca2_1$ in ORT) has been confirmed by the refinement of the structure. The symmetry operations for MLT

$$x, y, z; \; -x, \; -y + \tfrac{1}{2}, \; z + \tfrac{1}{2}$$

are modified from those given in *International Tables for X-ray Crystallography* (1956, Vol. I), in order to be in agreement with the results given in Lefebvre, Carpentier & Jakubas (1991) for both OHT and ORT phases. The Lorentz–polarization and spherical absorption corrections were applied. The structure was refined using *SHELX*76 (Sheldrick, 1976).

Starting atomic coordinates for the Bi and Cl atoms are those found in the ORT phase. After several cycles of refinement, a difference Fourier synthesis allows the determination of the atomic coordinates of the N and C atoms. The second equilibrium position for the C—N axis of all the methylammonium cations has not been found, which indicates that all the cations are ordered at this temperature. We were not able to localize the positions of the H atoms and they were neglected during the refinement of the structure. High peaks and holes on the residual electronic density of up to 1.77 and -2.35 e Å^{-3} were found near the Bi atoms at 130 K. We should remember that the same effect has been observed in ORT at 294 K. In comparison with the ORT phase, in the MLT phase the observed peaks and holes are nearly twice the value, because the spherical electronic density model becomes less and less valid with decreasing temperature. All the atoms were refined with anisotropic temperature factors. For further experimental details see Table 1.*

The inequivalent atoms of the unit cell with atom-numbering scheme are shown in Fig. 1. A list of the fractional atomic coordinates and equivalent isotropic temperature factors is given in Table 2 and bond lengths and angles are shown in Table 3. A projection of the structure along the b axis in the planes $y = 0$ and $y = \frac{1}{2}$ is shown in Figs. 2(*a*) and (*b*), respectively, using *PLUTO* (Motherwell & Clegg, 1978).

* Lists of structure factors and anisotropic thermal parameters have been deposited with the IUCr (Reference: PA9295). Copies may be obtained through The Managing Editor, International Union of Crystallography, 5 Abbey Square, Chester CH1 2HU, England.

Table 1. *Refinement parameters and experimental data*

Crystal data	
$[NH_3(CH_3)]_5Bi_2Cl_{11}$	Mo $K\alpha$ radiation
$M_r = 968.3$	$\lambda = 0.7107$ Å
Monoclinic	Cell parameters from 25 reflections
$P2_1$	$\theta = 7$–$20°$
$a = 12.880$ (4) Å	$\mu = 140.878$ cm^{-1}
$b = 13.916$ (3) Å	$T = 130$ K
$c = 15.059$ (5) Å	Spherical $r = 0.13$ mm
$\gamma = 90.13$ (2)°	$\mu r = 1.88$
$V = 2699$ (1) Å^3	Colorless
$Z = 4$	
Data collection	
$D_x = 2.383$ Mg m^{-3}	$\theta_{max} = 30°$
Enraf–Nonius CAD-4 diffractometer	$h = -18 \rightarrow 18$
	$k = 0 \rightarrow 19$
$\omega/2\theta$ scans	$l = 0 \rightarrow 21$
9592 measured reflections	3 standard refletions
5931 observed reflections	frequency = 60 min
$[I > 3\sigma(I)]$	intensity variation: −0.05% per h
Refinement	
Refinement on F	$\Delta\rho_{max} = 1.77$ e Å^{-3}
Weight = $1/[\sigma^2(F) + 0.000212.F^2]$	$\Delta\rho_{min} = -2.35$ e Å^{-3}
Final $R = 0.031$	Atomic scattering factors from *International Tables for X-ray Crystallography* (1974, Vol. IV)
$wR = 0.032$	
5931 reflections	
414 parameters	
H-atom parameters not refined	

3. Results and discussion

3.1. *Crystal structure of the low-temperature phase at* 130 K

Previous X-ray studies of PMACB by Lefebvre, Carpentier & Jakubas (1991) showed that the OHT →ORT phase transition is accompanied by a distinct

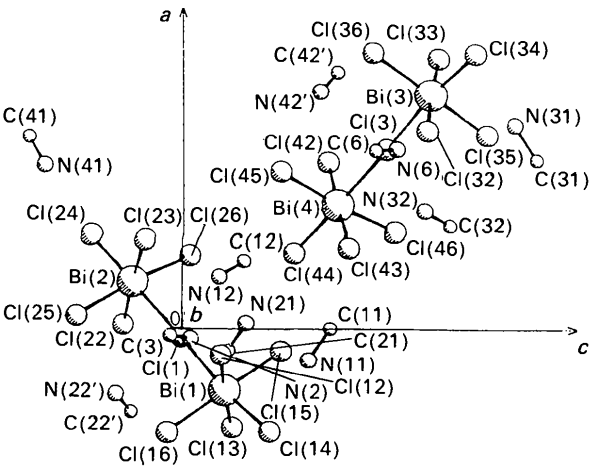

Fig. 1. Projections of the asymmetric unit with scheme-numbered atoms along the b axis.

Table 2. *Positional parameters* ($\times 10^4$) *and equivalent isotropic temperature factors* ($Å^2 \times 10^3$)

$U_{eq} = (1/3)\sum_i \sum_j U_{ij} a_i^* a_j^* \mathbf{a}_i . \mathbf{a}_j$.

	x	y	z	U_{eq}
Bi(1)	−1816 (1)	820 (1)	1062 (1)	16 (1)
Bi(2)	1415 (1)	−815 (1)	−1222 (1)	15 (1)
Cl(1)	−220 (2)	−6 (2)	−10 (2)	23 (2)
Cl(12)	−765 (2)	2539 (2)	974 (2)	21 (2)
Cl(13)	−2903 (2)	−780 (2)	1255 (2)	27 (2)
Cl(14)	−3034 (2)	1682 (2)	2168 (2)	25 (2)
Cl(15)	−647 (2)	331 (2)	2442 (2)	25 (2)
Cl(16)	−3053 (2)	1318 (2)	−351 (2)	23 (2)
Cl(22)	162 (2)	−2258 (2)	−1454 (2)	22 (2)
Cl(23)	2630 (2)	882 (2)	−917 (2)	19 (2)
Cl(24)	2774 (2)	−1460 (2)	−2256 (2)	36 (2)
Cl(25)	431 (2)	100 (2)	−2600 (2)	22 (2)
Cl(26)	2177 (2)	−1674 (2)	200 (2)	29 (2)
C(11)	23 (9)	2668 (9)	3641 (8)	28 (13)
N(11)	−920 (8)	2794 (6)	3113 (6)	24 (10)
C(21)	−620 (13)	−2399 (11)	1159 (12)	40 (19)
N(21)	190 (7)	−1806 (7)	1586 (7)	27 (10)
C(12)	2011 (11)	741 (9)	1527 (9)	33 (14)
N(12)	1551 (9)	1470 (7)	917 (6)	31 (11)
C(22′)	−2433 (10)	−1172 (8)	−1241 (10)	31 (14)
N(22′)	−1900 (8)	−353 (6)	−1630 (7)	24 (10)
C(3)	−167 (11)	5607 (9)	−290 (9)	38 (13)
N(3)	−268 (7)	4673 (7)	223 (7)	22 (10)
Bi(3)	6817 (1)	817 (1)	6061 (1)	14 (1)
Bi(4)	3585 (1)	−815 (1)	3778 (1)	14 (1)
Cl(3)	5220 (2)	−1 (2)	4989 (2)	17 (2)
Cl(32)	5763 (2)	2538 (2)	5976 (2)	21 (2)
Cl(33)	7886 (2)	−783 (2)	6254 (2)	27 (2)
Cl(34)	8037 (2)	1683 (2)	7170 (2)	18 (2)
Cl(35)	5642 (2)	330 (2)	7436 (2)	26 (2)
Cl(36)	8055 (2)	£317 (2)	4650 (2)	24 (2)
Cl(42)	4841 (2)	−2258 (2)	3548 (2)	25 (2)
Cl(43)	2369 (2)	881 (2)	4079 (2)	25 (2)
Cl(44)	2225 (2)	−1465 (2)	2750 (2)	22 (2)
Cl(45)	4574 (2)	95 (2)	2399 (2)	24 (2)
Cl(46)	2824 (2)	−1668 (2)	5197 (2)	27 (2)
C(31)	4935 (10)	2647 (8)	8655 (8)	34 (13)
N(31)	5946 (8)	2685 (7)	8115 (6)	29 (10)
C(41)	5611 (8)	−2405 (9)	6184 (9)	32 (13)
N(41)	4793 (8)	−1777 (9)	6572 (9)	33 (13)
C(32)	3002 (10)	734 (9)	6525 (9)	38 (14)
N(32)	3436 (7)	1470 (6)	5914 (6)	21 (10)
C(42′)	7475 (9)	−1188 (8)	3780 (10)	28 (13)
N(42′)	6902 (7)	−352 (7)	3361 (7)	25 (10)
C(6)	5179 (11)	6678 (10)	4713 (9)	43 (15)
N(6)	5222 (8)	4659 (7)	5232 (7)	27 (10)

Table 3. *Bond lengths* (Å) *and angles* (°) *in PMACB in the low-temperature phase* $T = 130$ K

(*a*) Bond lengths

Bi(1)—Cl(1)	2.857 (3)	Bi(3)—Cl(3)	2.851 (3)
Bi(1)—Cl(12)	2.750 (3)	Bi(3)—Cl(32)	2.756 (3)
Bi(1)—Cl(13)	2.642 (3)	Bi(3)—Cl(33)	2.639 (3)
Bi(1)—Cl(14)	2.586 (3)	Bi(3)—Cl(34)	2.587 (3)
Bi(1)—Cl(15)	2.656 (3)	Bi(3)—Cl(35)	2.653 (3)
Bi(1)—Cl(16)	2.748 (3)	Bi(3)—Cl(36)	2.745 (3)
Bi(2)—Cl(1)	3.008 (3)	Bi(4)—Cl(3)	3.006 (3)
Bi(2)—Cl(22)	2.597 (3)	Bi(4)—Cl(42)	2.603 (3)
Bi(2)—Cl(23)	2.867 (3)	Bi(4)—Cl(43)	2.872 (3)
Bi(2)—Cl(24)	2.510 (3)	Bi(4)—Cl(44)	2.504 (3)
Bi(2)—Cl(25)	2.747 (3)	Bi(4)—Cp(45)	2.744 (3)
Bi(2)—Cl(26)	2.641 (3)	Bi(4)—Cl(46)	2.633 (3)
C(11)—N(11)	1.453 (15)	C(31)—N(31)	1.536 (16)
C(21)—N(21)	1.475 (19)	C(41)—N(41)	1.490 (16)
C(12)—N(12)	1.494 (16)	C(32)—N(32)	1.485 (16)
C(22′)—N(22′)	1.453 (15)	C(42′)—N(42′)	1.517 (15)
C(3)—N(3)	1.517 (16)	C(6)—N(6)	1.500 (17)

(*b*) Bond angles

Cl(1)—Bi(1)—Cl(12)	88.3 (1)	Cl(3)—Bi(3)—Cl(32)	88.0 (1)
Cl(1)—Bi(1)—Cl(13)	95.9 (1)	Cl(3)—Bi(3)—Cl(33)	95.8 (1)
Cl(1)—Bi(1)—Cl(14)	171.3 (1)	Cl(3)—Bi(3)—Cl(34)	171.2 (1)
Cl(1)—Bi(1)—Cl(15)	86.0 (1)	Cl(3)—Bi(3)—Cl(35)	85.9 (1)
Cl(1)—Bi(1)—Cl(16)	94.7 (1)	Cl(3)—Bi(3)—Cl(36)	94.7 (1)
Cl(12)—Bi(1)—Cl(13)	175.6 (1)	Cl(32)—Bi(3)—Cl(33)	175.8 (1)
Cl(12)—Bi(1)—Cl(14)	85.7 (1)	Cl(32)—Bi(3)—Cl(34)	85.8 (1)
Cl(12)—Bi(1)—Cl(15)	89.0 (1)	Cl(22)—Bi(3)—Cl(35)	88.7 (1)
Cl(12)—Bi(1)—Cl(16)	91.6 (1)	Cl(33)—Ni(3)—Cl(36)	91.8 (1)
Cl(13)—Bi(1)—Cl(14)	90.0 (1)	Cl(33)—Bi(3)—Cl(34)	90.2 (1)
Cl(13)—Bi(1)—Cl(15)	89.9 (1)	Cl(33)—Bi(3)—Cl(35)	89.7 (1)
Cl(13)—Bi(1)—Cl(16)	89.5 (1)	Cl(33)—Bi(3)—Cl(36)	89.7 (1)
Cl(14)—Bi(1)—Cl(15)	87.7 (1)	Cl(34)—Bi(3)—Cl(35)	87.8 (1)
Cl(14)—Bi(1)—Cl(16)	91.7 (1)	Cl(34)—Bi(3)—Cl(36)	91.7 (1)
Cl(15)—Bi(1)—Cl(16)	179.1 (1)	Cl(35)—Bi(3)—Cl(36)	179.3 (1)
Cl(1)—Bi(2)—Cl(22)	86.3 (1)	Cl(3)—Bi(4)—Cl(42)	86.3 (1)
Cl(1)—Bi(2)—Cl(23)	88.6 (1)	Cl(3)—Bi(4)—Cl(43)	88.7 (1)
Cl(1)—Bi(2)—Cl(24)	178.8 (1)	Cl(3)—Bi(4)—Cl(44)	178.9 (1)
Cl(1)—Bi(2)—Cl(25)	87.7 (1)	Cl(3)—Bi(4)—Cl(45)	87.8 (1)
Cl(1)—Bi(2)—Cl(26)	86.5 (1)	Cl(3)—Bi(4)—Cl(46)	86.4 (1)
Cl(22)—Bi(2)—Cl(23)	174.5 (1)	Cl(42)—Bi(4)—Cl(43)	174.6 (1)
Cl(22)—Bi(2)—Cl(24)	94.2 (1)	Cl(42)—Bi(4)—Cl(44)	94.3 (1)
Cl(22)—Bi(2)—Cl(25)	88.3 (1)	Cl(42)—Bi(4)—Cl(45)	88.1 (1)
Cl(22)—Bi(2)—Cl(26)	89.4 (1)	Cl(42)—Bi(4)—Cl(46)	89.5 (1)
Cl(23)—Bi(2)—Cl(24)	90.8 (1)	Cl(43)—Bi(4)—Cl(44)	90.7 (1)
Cl(23)—Bi(2)—Cl(25)	89.4 (1)	Cl(43)—Bi(4)—Cl(45)	89.6 (1)
Cl(23)—Bi(2)—Cl(26)	92.4 (1)	Cl(43)—Bi(4)—Cl(46)	92.2 (1)
Cl(24)—Bi(2)—Cl(25)	91.2 (1)	Cl(44)—Bi(4)—Cl(45)	91.3 (1)
Cl(24)—Bi(2)—Cl(26)	94.7 (1)	Cl(44)—Bi(4)—Cl(46)	94.5 (1)
Cl(25)—Bi(2)—Cl(26)	173.9 (1)	Cl(45)—Bi(4)—Cl(46)	173.9 (1)
Bi(1)—Cl(1)—Bi(2)	176.9 (1)	Bi(3)—Cl(3)—Bi(4)	177.1 (1)

distortion of $Bi_2Cl_{11}^{5-}$ anions. The shift between the center of mass of the ion and the bridging Cl(1) atom amounts to 0.089 Å in ORT, whereas the estimated value from the present results is 0.083 Å. The deformation of the bioctahedra units can also be deduced from the results presented by Lefebvre, Carpentier & Jakubas (1991) (see Table 3) for ORT and in Table 3 for MLT. The bond angles vary between 85.8–95.9° and 171.2–179.3° at 130 K and are similar to those obtained at 294 K. This indicates that in spite of a wide temperature range of more than 150 K, we could not observe any change in this type of distortion. This distortion of the $BiCl_6$ octahedra and the residual electronic density found near the Bi atoms can be explained by the 'inert pair effect'. The lone pair ($6s^2$) of the Bi^{3+} ion (aspherical symmetrical orbital) is stereochemically active and may cause a distortion of the octahedral coordination environment. On the other hand, a noticeable evolution in the "torsion angle" of the bioctahedron unit is revealed with decreasing temperature. The torsion angle may be defined as an angle between two planes containing three atoms, *e.g.* Bi(1), Bi(2), Cl(12) and Bi(1), Bi(2), Cl(23) for ORT and also Bi(3), Bi(4), Cl(32) or Bi(3), Bi(4), Cl(43) for the MLT. For this case, the following sequence has been recorded: OHT (at 349 K) $\varphi_1 \approx 1°$, ORT (at 294 K) $\varphi_1 = 5.96°$, MLT (130 K) $\varphi_1 = 12.3$ and 15.53°. The remaining three angles defined in the same way (φ_2, φ_3 and φ_4) are comparable to the φ_1. One can now state that within the temperature range 307–130 K, we are dealing with the rotation of two octahedra, to

each other, around the Bi(1)—Cl(1)—Bi(2) axis without any distortion (see Fig. 3). This rotation probably develops continuously over this temperature range.

The hydrogen-bonded $[NH_3(CH_3)]^+$ ions (all types) with their ordered C—N axes are a characteristic feature of the MLT phase at 130 K. Since ten different methylammonium cations exist in the unit cell, the observed hydrogen-bond system is rather complex. Table 4 lists the N···Cl distances corresponding to possible hydrogen bonds shorter than 3.42 Å. On comparing the ORT and MLT phases, it should be noted that most of the hydrogen bonds existing at 294 K become a little shorter at 130 K and more importantly, many new hydrogen bonds appear involving $[NH_3(CH_3)]^+$ cations of type (2) in the MLT phase. In our opinion, the present hydrogen-bond system is crucial for stabilizing the position of the methylammonium cations. An interesting feature in the structure at 130 K is found for MA(12). The shortest hydrogen bonds (below 3.25 Å) of this cation are oriented along the polar *c* axis, as also observed for MA(3) in the ferroelectric phase (ORT), suggesting that the dipole moment of such NH···Cl bonds may contribute to the polar properties of the crystal. It is essential to stress that the N···Cl contact distances (3.1–3.3 Å) of the PMACB crystal at low temperatures are consistent with those encountered in a number of methylammonium salts with weak N—H···Cl hydrogen bonding (Chapuis, Arend & Kind, 1975; Chapuis, Kind & Arend, 1976).

Table 4. *Selected* Cl···N *distances* (Å)

N(11)···Cl(23)	3.036	N(31)···Cl(16)	3.259
N(11)···Cl(12)	3.235	N(31)···Cl(32)	3.237
N(11)···Cl(36)	3.280	N(31)···Cl(34)	3.353
N(11)···Cl(25)	3.312	N(31)···Cl(43)	3.284
N(21)···Cl(26)	3.307	N(31)···Cl(45)	3.343
N(21)···Cl(44)	3.189	N(41)···Cl(24)	3.175
N(21)···Cl(15)	3.418	N(41)···Cl(35)	3.387
N(12)···Cl(34)	3.231	N(41)···Cl(46)	3.278
N(12)···Cl(12)	3.337	N(41)···Cl(42)	3.300
N(12)···Cl(23)	3.199	N(32)···Cl(3)	3.381
N(12)···Cl(1)	3.369	N(32)···Cl(32)	3.345
N(22′)···Cl(1)	3.297	N(32)···Cl(43)	3.192
N(22′)···Cl(16)	3.367	N(32)···Cl(14)	3.233
N(22′)···Cl(25)	3.396	N(42′)···Cl(13)	3.238
N(22′)···Cl(33)	3.253	N(42′)···Cl(14)	3.353
N(22′)···Cl(34)	3.362	N(42′)···Cl(3)	3.308
N(3)···Cl(12)	3.214	N(42′)···Cl(36)	3.369
N(3)···Cl(25)	3.300	N(42′)···Cl(45)	3.389
N(3)···Cl(36)	3.284	N(6)···Cl(32)	3.234
N(3)···Cl(43)	3.298	N(6)···Cl(16)	3.226
		N(6)···Cl(23)	3.352
		N(6)···Cl(45)	3.291

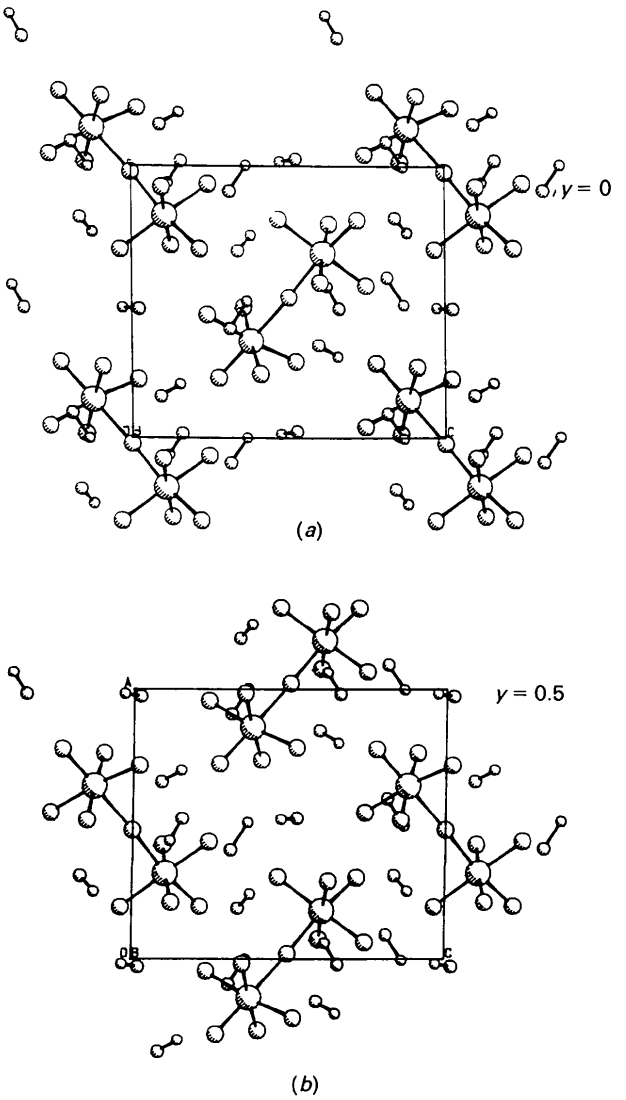

Fig. 2. Projections of the unit-cell contents along the *b* axis, (*a*) at $y = 0$ and (*b*) at $y = 0.5$.

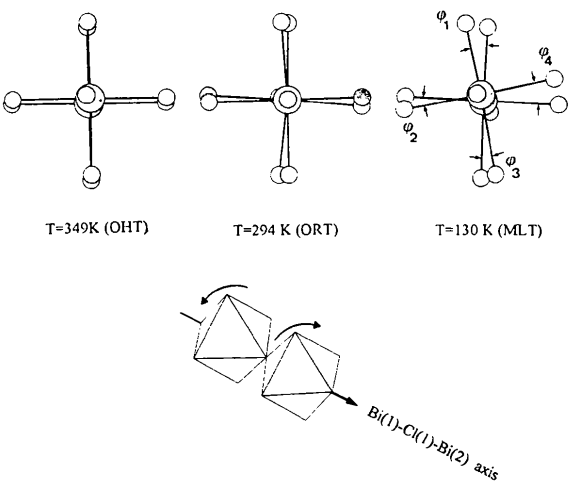

Fig. 3. Evolution in the torsional angle of the bioctahedral unit ($Bi_2Cl_{11}^{5-}$) in different phases.

3.2. *Change in cell dimensions with temperature*

We should underline that refinement of the structure (at 130 K) and temperature measurement (unit-cell parameters and evolution of the monoclinic angle) were performed on two different single crystals. The values of these parameters for the two crystals exhibit some small differences, but within experimental error.

Fig. 4 shows the variations of the cell dimensions in the low-temperature region. The cell volume and the volumic thermal expansion coefficient against temperature are presented in Fig. 5. The temperature evolution of these parameters is characterized by a distinct anisotropy in the thermal properties. In the low-temperature region between 270 and 100 K, the thermal expansion coefficient for the *a*-axis changes its sign twice around 210 and 130 K, but the value of the *a* parameter at 100 and 270 K is almost the same.

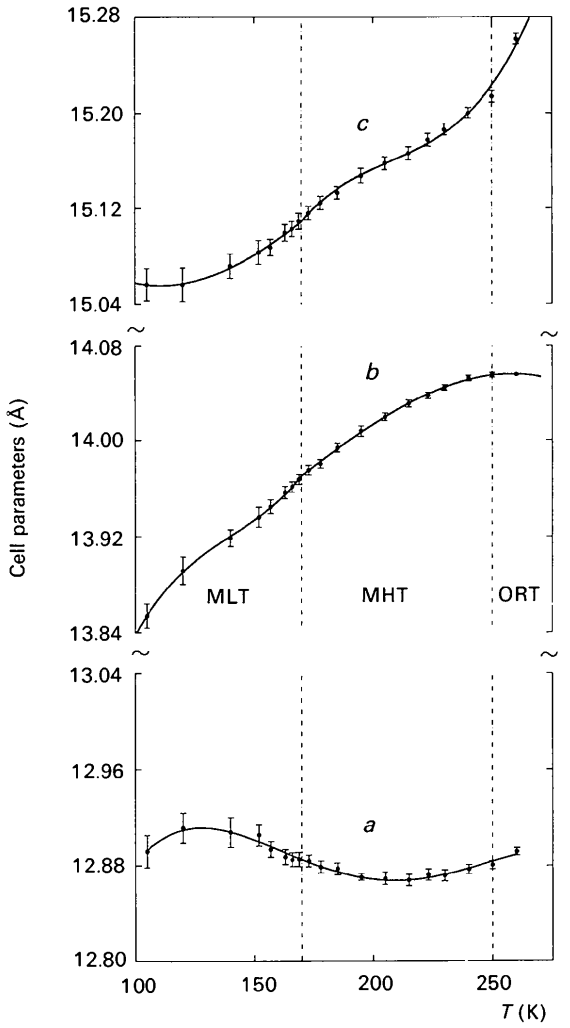

Fig. 4. Temperature dependence of the unit-cell parameters of $[NH_3(CH_3)]_5Bi_2Cl_{11}$ in the low-temperature region.

The *b*-direction reveals a broad maximum around 255 K, whereas *c* shows a noticeable non-linearity within the studied temperature region. For the *b*- and *c*-axes, only subtle anomalies are visible as the gradient (db/dT, dc/dT) changes near 170 K. The volume expansion (see Fig. 5) shows similar phenomena around the 170 K phase transition (PT) region. We should notice that the volume expansion coefficient [$\alpha = (1/V)(dV/dT)$] displays a small discontinuity near 170 K. The observed anisotropy in the thermal expansion and relatively large thermal expansion coefficients of the order $10^{-4}\,K^{-1}$ along the *b*- and *c*-axes can justify both the distortion of the anionic sublattice ($Bi_2Cl_{11}^{5-}$) and the appearance of the monoclinic angle in the low-temperature region.

3.3. *Temperature evolution of the monoclinic angle from X-ray measurements*

Fig. 6. shows the temperature evolution of a monoclinic angle in the low-temperature region. It is clearly seen that γ is different from 90°, starting from 250 ± 10 K, and the changes seem to be continuous. This study proved that PMACB undergoes a phase transition from the orthorhombic to the monoclinic system at this temperature. The monoclinic phase, which exists in the temperature range 170–250 K, is noted in the text as a monoclinic high-temperature phase (MHT). We should remember that the structure at 130 K revealed great similarity with the ORT phase (294 K), which implies that the expected difference in the structures of ORT and MHT is so subtle that the ORT–MHT phase transition is practically invisible by most experimental techniques. The change in spontaneous polarization below 250 K is the only experimental evidence which may confirm the presence of such phase transitions.

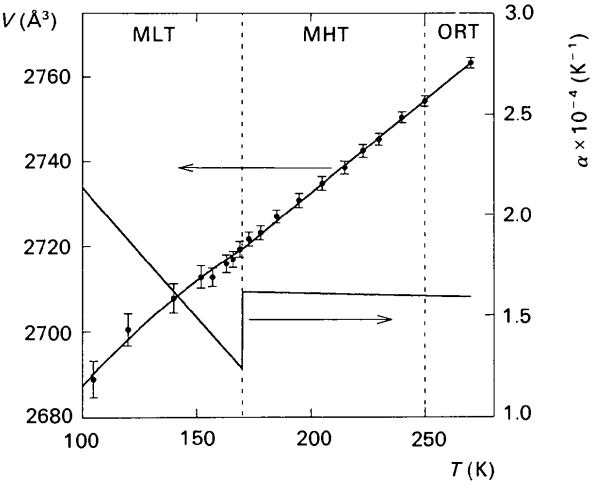

Fig. 5. The volume of the unit cell and the volume expansion coefficient (α) of $[NH_3(CH_3)]_5Bi_2Cl_{11}$ as a function of temperature.

According to the Landau theory, the continuous ORT→MHT phase transition is possible only with a change in space group ($Pca2_1 \rightarrow P2_1$ in the present case). Such a phase transition indicates that this material is probably ferroelastic in the monoclinic phases (Sapriel, 1975). When the 170 K phase transition is crossed, the monoclinic angle does not reveal any noticeable anomaly.

The lowest temperature transition MHT→MLT at *ca* 170 K is suggested to occur between two phases having the same symmetry; such a phase transition is known as an 'equisymmetric' transition, which has been reported for many crystals (*e.g.* Banerjee, Nath & Chaudhuri, 1982; Belkyal, Mokhlisse, Tanouti, Chanh & Couzi, 1993; Aizu, 1985).

3.4. *The mechanism of the phase transitions*

The sequence of the phase transitions in PMACB with decreasing temperature may only be explained by changes in the motion of the polar $[NH_3(CH_3)]^+$ groups. The $[NH_3(CH_3)]^+$ ion has a permanent dipole moment, thus a dynamical process changing the orientation of this ion should contribute to the spontaneous polarization of PMACB. The temperature dependence of the spontaneous polarization in a wide temperature range (Mroz & Jakubas, 1990) with the contribution of different types of methylammonium cations to ΔP_s is illustrated in Fig. 7. In order to propose the mechanism of the phase transition it is necessary to consider the evolution of the motional state of these cations over all the phases. The evolution of the probability for the two-sites position model to describe the disordering of MA cations in the successive phases is represented schematically in Table 5 ($p = 1$ indicates that MA is completely ordered, whereas for $p = 0$ the position of such a cation is not observed). According to the crystallographic symmetry, two equivalent cations in the OHT phase generate two inequivalent cations in the ORT phase and each cation of the ORT phase generates two inequivalent cations both in the MHT and MLT modifications. The relation between the corresponding ions is marked by an arrow.

As shown in the diagram, the para-ferroelectric OHT–ORT phase transition is accompanied by a change in the motional state of both the MA(3) and MA(2) cations. Taking into account the changes in the value of the probability when the 307 K PT is crossed, it is clear that both types of these cations contribute to ΔP_{s1} below 307 K, but MA(3) is dominant and becomes practically ordered at 294 K. We should notice that in the case of the MA(2) cations, which are inequivalent in ORT, their contribution to ΔP_{s1} is comparable ($\Delta p \approx 0.2$), but for MA(12) one of two possible positions becomes distinctly preferred ($p_{21} = 0.84$) just before reaching the plateau of the P_s (T) curve. In the temperature range 280–250 K, P_s maintains the same value, which implies that we cannot expect any change in the disordering of MA cations of type (2). Below 250 K P_s increases, showing an inflection point at *ca* 170 K and at 130 K, P_s is nearly saturated. Now it is necessary to consider the hydrogen-bond system (in MLT) to estimate how the strength of the N—H···Cl hydrogen bond influences the evolution of the disordering of MA cations below 250 K. Taking the N—H···Cl distances from Table 5 at 130 K (the N—H···Cl angle is neglected), we can see that MA(12) is stabilized by two bonds of 3.199 and 3.231 Å, whereas MA(22) is hydrogen bonded by only one comparable bond of 3.189 Å. Taking into account these lengths and the fact that MA(12) is close to the ordered state below 280 K, it is evident that this type of cation

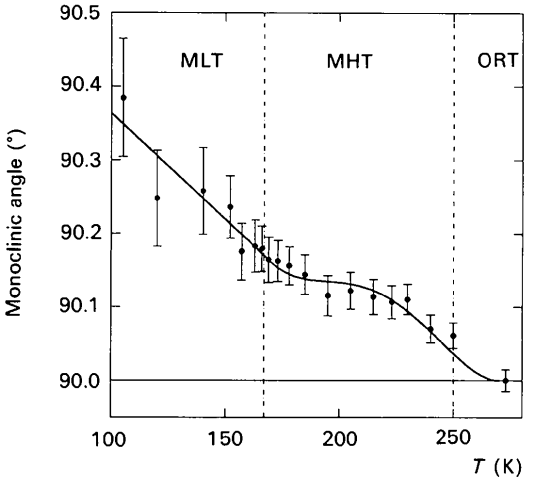

Fig. 6. Temperature dependence of the monoclinic angle (γ) for $[NH_3(CH_3)]_5Bi_2Cl_{11}$.

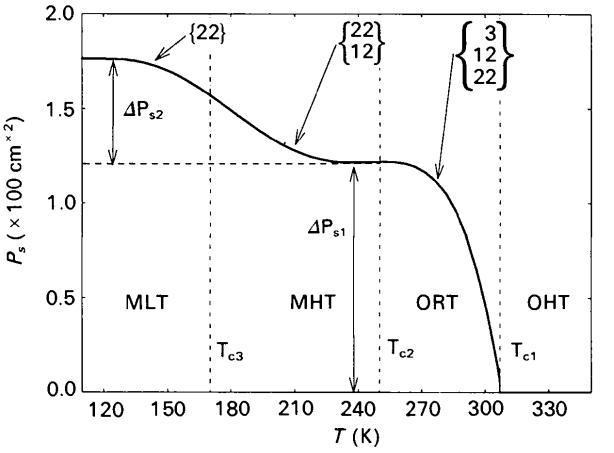

Fig. 7. Scheme illustrating the successive contribution of the methylammonium cations to the spontaneous polarization over the polar phases of $[NH_3(CH_3)]_5Bi_2Cl_{11}$.

Table 5. *Schematic representation of the disorder of the methylammonium cations in all phases of PMACB*

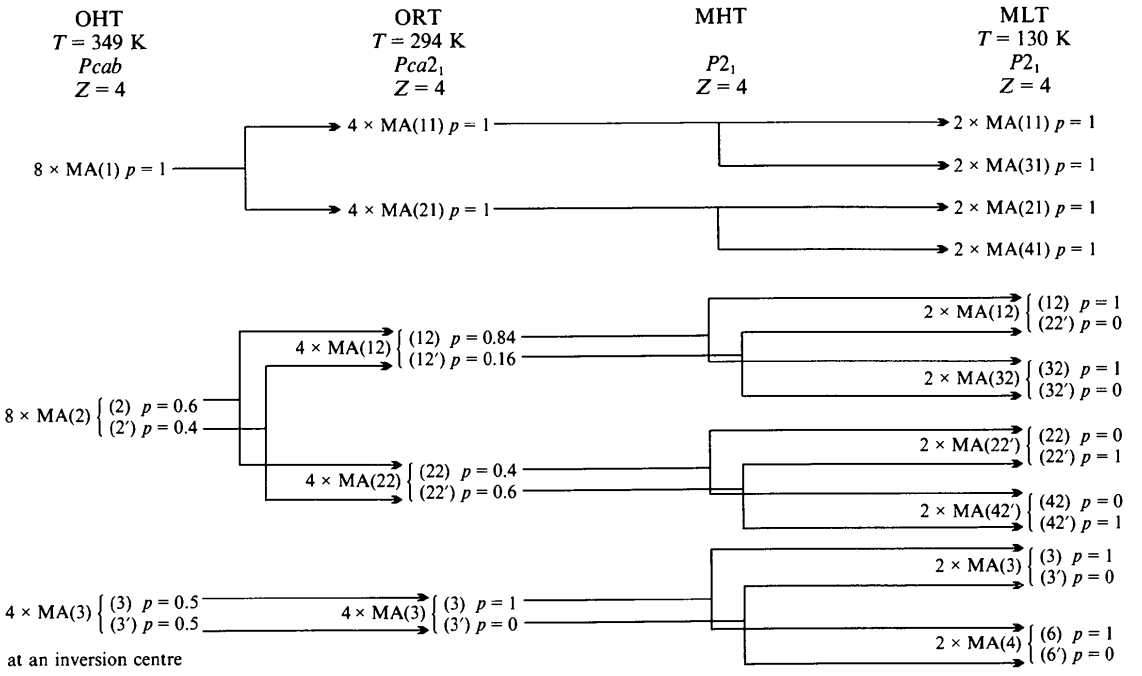

MA(i) methylammonium cation of type *i*, (*i*) and (*i*′) note the two different positions of the same cation and *p* is the probability for each position; *n* × MA indicates that *n* equivalent cations exist in the unit cell (the total number of MA cations is 20).

should be fully ordered before MA(22). We suggest that MA(12) contributes mainly to ΔP_{s2} below 250 K and becomes completely ordered before reaching the postulated phase transition around 170 K. Finally the MA(22) cations play the main role through the 170 K PT. The saturation of P_s below 130 K is strictly related to the fully ordered state of MA(22).

4. Concluding remarks

(1) The structural analysis of the title compound at 130 K indicated that the MLT phase ($\gamma = 90.13°$) is close to the orthorhombic system (ORT) and the differences in the structure of both phases are very subtle.

(2) In the lowest temperature phase (at 130 K), the C—N axes of all methylammonium cations are completely ordered.

(3) Temperature-dependent X-ray studies show that PMACB displays subtle and continuous transitions from the orthorhombic to the monoclinic system ($Pca2_1 \rightarrow P2_1$) at a temperature of *ca* 250 ± 10 K.

(4) The proposed model of disordering of the methylammonium cations based on the structural analyses at three different temperatures (in OHT, ORT and MLT phases) is consistent with temperature evolution of the spontaneous polarization. According to this, the MA(12) cation contributes to the ORT→MHT transition whereas MA(22) plays the main role in the mechanism of the postulated phase transition around 170 K.

(5) If an anomaly exists at $T = 170$ K, on the other hand, it is not evident that this corresponds to a second-order phase transition, because of the small discontinuity of α. It can also be interpreted as a continuous structural evolution. This structural anomaly around 170 K found by other experimental techniques has been interpreted as an 'equisymmetric' transition.

(6) The possible sequence of the phase transitions in PMACB is presented below:

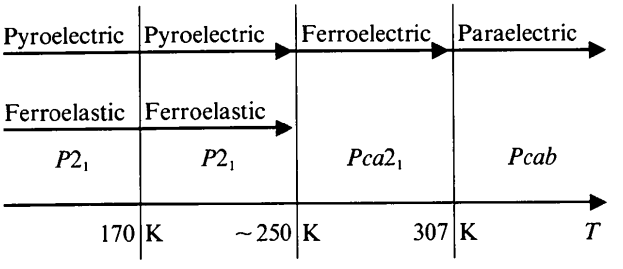

References

AIZU, K. (1985). *J. Phys. Soc. Jpn*, **54**, 203–210.

BELKYAL, I., MOKHLISSE, R., TANOUTI, B., CHANH, N. B. & COUZI, M. (1993). *Phys. Status Solidi A*, **136**, 45–56.

BANERJEE, S., NATH, D. & CHAUDHURI, B. K. (1982). *Phys. Rev. B*, **25**, 1883–1891.
CARPENTIER, P., LEFEBVRE, J. & JAKUBAS, R. (1992). *J. Phys. Condens. Matter*, **4**, 2985–2999.
CHAPUIS, G., AREND, H. & KIND, R. (1975). *Phys. Status Solidi*, **31**, 449–462.
CHAPUIS, F., KIND, R. & AREND, H. (1976). *Phys. Status Solidi*, **36**, 285–295.
IWATA, M. & ISHIBASHI, Y. (1990). *J. Phys. Soc. Jpn*, **59**, 4239–4242.
IWATA, M. & ISHIBASHI, Y. (1992). *J. Phys. Soc. Jpn*, **61**, 4615–4618.
JAKUBAS, R. & SOBCZYK, L. (1990). *Phase Transit.* **20**, 163–193.
JAKUBAS, R., SOBCZYK, L. & LEFEBVRE, J. (1989). *Ferroelectrics*, **100**, 143–149.
KUOK, M. H., NG, S. C., IWATA, M. & ISHIBASHI, Y. (1993). *Solid State Commun.* **86**, 151–154.
LEFEBVRE, J., CARPENTIER, P. & JAKUBAS, R. (1991). *Acta Cryst.* B**47**, 228–234.
MOTHERWELL, W. D. S. & CLEGG, W. (1978). *PLUTO. Program for Plotting Molecular and Crystal Structures.* Univ. of Cambridge, England.
MROZ, J. & JAKUBAS, R. (1990). *Ferroelectr. Lett.* **11**, 53–56.
PAWLACZYK, C., JAKUBAS, R., PLANTA, K., BRUCH, C., STEPHAN, J. & UNRUH, H. G. (1992). *Ferroelectrics*, **126**, 145–150.
PAWLOWSKI, A., RAMOS, S. & CERRO, J. (1993). Abstract of the 8th IMF, Gaithersburg, USA.
SAPRIEL, J. (1975). *Phys. Rev.* **12**, 5128–5140.
SHELDRICK, G. M. (1976). *SHELX76. Program for Crystal Structure Determination.* Univ. of Cambridge, England.

Acta Cryst. (1995). B**51**, 174–177

Structure of $C_{36}H_{52}Cl_6InN_3O_{14}$ Determined by Nonlinear Least Squares

BY R. SPENGLER, J. LANGE, H. ZIMMERMANN AND H. BURZLAFF

Institut für Angewandte Physik, Lehrstuhl für Kristallographie, Bismarckstrasse 10, 91054 *Erlangen, Germany*

AND P. G. VELTSISTAS AND M. I. KARAYANNIS

Department of Analytical Chemistry, University of Ioannina, Greece

(*Received* 12 *March* 1994; *accepted* 20 *May* 1994)

Abstract

Tris(triethylammonium) tris[3,6-dichloro-4,5-dihydroxy-3,5-cyclohexadiene-1,2-dionato(2−)]indium dihydrate, $[C_6H_{16}N]_3[In(C_6Cl_2O_4)_3].2H_2O$, $M_r = 1078.36$, orthorhombic, $Pbcn$, $a = 26.639$ (4), $b = 16.667$ (2), $c = 10.538$ (2) Å, $V = 4678.6$ (5) Å, $Z = 4$, $D_x = 1.540$ g cm^{-3}, λ(Mo $K\alpha$) = 0.70926 Å, $\mu = 0.9087$ mm^{-1}, $F(000) = 2208$, room temperature, final $R(F) = 0.061$ for 2551 reflections. The structure could only be determined using least-squares with the Levenberg–Marquardt algorithm, including the second derivatives of the structure factors. A refinement with standard least-squares stopped at an R-value of 16%, but showed stability with the Levenberg–Marquardt result.

Introduction

This investigation is the third in a series studying the behavior of different metals in anilates. The data showed problems in the refinement of the structure, caused by statistical distribution of one of the cations. Within the scope of a project working with structures showing pseudosymmetry, a recently developed least-squares program using the Levenberg–Marquardt algorithm improved the refinement procedure and led to the final solution of the structure.

Synthesis of the compound

A suspension of the hydrated indium(III)hydroxide was digested in a water bath with a stoichiometric excess of solid chloranilic acid for *ca* 3 h, until the reaction was complete and the reagents thoroughly disappeared. The hydroxide was fully dissolved, while the excess acid remained as a solid.

Into this solution, the exact quantity of triethylamine free base was introduced stepwise in small portions, under continuous stirring. After full neutralization of the excess chloranilic acid, the final pH reached the range 7–8. The mixture was then slowly heated in a water bath, filtered and received in a mixture of acetone–ethanol with strong stirring. A lilac–violet crystalline complex salt was well separated with a yield of *ca* 70%.

The crystalline product was filtered, first washed with a mixture of ethanol–ether and finally with ether. The crystals were dried under an air stream and finally under vacuum in the presence of phosphorus pentoxide for 24 h. They were recrystallized from DMSO by the addition of absolute ethanol, giving long gray–violet crystals.

Experimental

All measurements were performed on a rebuilt PW 1100 instrument (Gomm, 1993). Crystal dimensions

©1995 International Union of Crystallography
Printed in Great Britain – all rights reserved